RASĀYAN *J. Chem.*
Vol. 19 | No. 4 | 1984-1992 | October-December | 2026
ISSN: 0974-1496 | e-ISSN: 0976-0083 | CODEN: RJCABP
http://www.rasayanjournal.com
http://www.rasayanjournal.co.in

ECO-FRIENDLY SYNTHESIS OF MAGNETITE NANOPARTICLES USING *Oxalis stricta* LEAF EXTRACT: CHARACTERIZATION, ANTI-FUNGAL AND PHOTOCATALYTIC APPLICATIONS

B. Lavanya✉ and Y. Aparna
Department of Physics, Jawaharlal Nehru Technological University Hyderabad, Telangana,500085, India
✉Corresponding author: lavanyabandari1@gmail.com

ABSTRACT

This study investigated the eco-friendly synthesis of iron oxide nanoparticles (Fe_3O_4 NPs) using *Oxalis stricta* leaf (OSL) extract. The Fe_3O_4 NPs were characterised using XRD, FESEM, FTIR, UV-Vis, and PL. XRD analysis revealed a cubic, crystalline phase with a crystallite size of 14.37 nm. FESEM images showed a rough, cauliflower-like surface morphology, with particle sizes ranging from 100 - 120 nm. FTIR spectra indicated the presence of various functional groups, confirming the formation and stabilisation of Fe_3O_4 NPs by phytochemicals in the OSL extract. UV-Vis spectroscopy showed a peak at 397 nm, and the energy band gap was calculated to be 2.77 eV using a Tauc plot. The antifungal activity of the Fe_3O_4 NPs was evaluated against Aspergillus niger and Trichoderma asperellum, with inhibition zones observed at concentrations starting from 125 µg/mL. The photocatalytic activity of Fe_3O_4 NPs was investigated for the degradation of methylene blue dye under UV radiation, and pseudo-first-order kinetics were observed. The results show that *Oxalis stricta*-mediated synthesis is a simple, environmentally friendly, sustainable method for producing functional Fe_3O_4 nanoparticles that possess antifungal and photocatalytic properties. The study contributes to ongoing research in green nanotechnology by presenting an environmentally friendly approach to the production of multifunctional nanomaterials whose applications include environmental remediation, wastewater treatment, and antimicrobial technologies, while laying the foundation for future studies on the sustainable production of nanomaterials.

Keywords: Green Synthesis, Iron Oxide Nanoparticles, *Oxalis Stricta*, Photocatalysis, Antimicrobial Activity.
RASĀYAN *J. Chem.*, Vol. 19, No.4, 2026

INTRODUCTION

Nanotechnology research has advanced rapidly over the past few years. These nanomaterials are composed of nanoparticles (NPs) smaller than 100 nm, which have numerous applications in biomedicine, environmental bioremediation, energy storage, and many other fields. These increasing applications are contributing to a change in the main intention of research toward promoting the evolution of viable and environmentally friendly inventions.[1] Nowadays, research has focused on the synthesis of metal nanoparticles (NPs) (such as Cu, Ag, Pt, Au, Mg, and Zn) and metal oxides (such as ZnO, TiO_2, CuO, and Ag_2O), etc., using green methods, which have shown potent benefits in different fields.[2-4] Among these metal oxide nanoparticles, iron oxides are the most beneficial because of their advantageous physical properties, such as superparamagnetic behaviour, low oxidation susceptibility, long blood half-lives, and variable surface chemistry. Additionally, they have numerous applications in biomedicine, medication delivery, magnetic cell sorting, magnetic resonance imaging (MRI), bioengineering, cosmetics, biosensing, and antimicrobial activity against various pathogens.[5,6] In the synthesis of Fe_3O_4 nanoparticles, different leaf extracts and peels were used.[7-12.] In this study, iron oxide nanoparticles were synthesised using *Oxalis stricta* (OS) leaf extract. *Oxalis stricta* is rich in compounds such as isovaledione, citric acid, flavones, glycoflavones, and phenolic acids. These specific phytochemicals, particularly flavones and phenolic acids, are known for their strong reducing and capping abilities, which are crucial for the efficient reduction of metal ions and stabilisation of nascent nanoparticles. This study hypothesises that the unique synergistic action of these compounds in *Oxalis stricta leaf* extract could lead to the synthesis of highly stable, functionally active Fe_3O_4 NPs with distinct properties. This type of oxalis leaf has a

range of colours from light pink to pale green.[14] The present study relates to Sustainable Development Goal (SDG) 3, Good Health and Well-Being, in which environmentally friendly green synthesis methods were developed for the preparation of magnetite (Fe_3O_4) antibacterial nanoparticles using *Oxalis stricta* leaf extract. To the best of our knowledge, the leaf extract of OS as a natural reducing and stabilising agent for synthesising magnetite (Fe_3O_4) nanoparticles has not been investigated, despite many plant extracts being reported in the literature for the green synthesis of magnetite nanoparticles.[15,16,17] Moreover, most earlier studies have focused on synthesising nanoparticles or on a single functional application, and there are few comprehensive studies of their structures and associated antibacterial and photocatalytic activities. Thus, a sustainable synthesis protocol using the leaf extract of *Oxalis stricta* is needed, and a systematic study of the physicochemical properties and multifunctional utilisation of the Fe_3O_4 nanoparticles is desired. To fill this gap, the present study aims to synthesise green Fe_3O_4 nanoparticles, investigate their structural and optical characteristics, and evaluate their antibacterial and photocatalytic efficiency, offering insights into their potential applications in environmental and biomedical fields.

EXPERIMENTAL

Materials, Methods and Preparation of Plant Extracts

Oxalis stricta leaves were collected from the garden located within the Anurag University campus in Hyderabad, Telangana, India. The gathered leaves were stored in an airtight container until use in the synthesis process. Ferric nitrate nano-hydrate ($Fe(NO_3)_3.9H_2O$) was purchased from Sigma-Aldrich Chemicals. Fe_3O_4 was synthesised using distilled water. Ethanol was used as the solvent.

Oxalis stricta leaves were collected from a nearby garden, washed under running water 2-3 times, then with distilled water 3 times to remove dust particles. After washing, the leaves were air-dried to remove moisture. The dried leaves were sliced into small pieces. Thirty grams of chopped leaves were soaked in 150 mL of distilled water in a 250 mL conical flask and heated at 80 °C for 30–40 min with continuous stirring on a magnetic stirrer. Finally, the final extract was allowed to cool, filtered through Watt–Mann filter paper, and centrifuged to remove any remaining plant residues. The final extract was stored at 4 ℃ and used for further synthesis.[18]

Synthesis of Iron Oxide Nps

To synthesise iron oxide nanoparticles, 40 mL of plant extract was placed in a 100 mL beaker, and four grams of ferric nitrate nonahydrate ($Fe(NO_3)_3.9H_2O$) was added to the plant extract. The resultant mixture was then heated at 60 ℃ for 1 h 30 min under continuous stirring on a magnetic stirrer. The colour of the mixture changed from light yellow to red-brown, indicating the formation of iron oxide nanoparticles. Before sample collection, the reaction mixture was centrifuged 3 times and washed with ethanol to remove impurities.[19] The procedure followed in the synthesis process is shown in Fig.-1(a). The mechanism involved reduction, oxidation, nucleation, growth and stabilisation, which results in the formation of Fe_3O_4 nanoparticles as shown in Fig.-1(b).

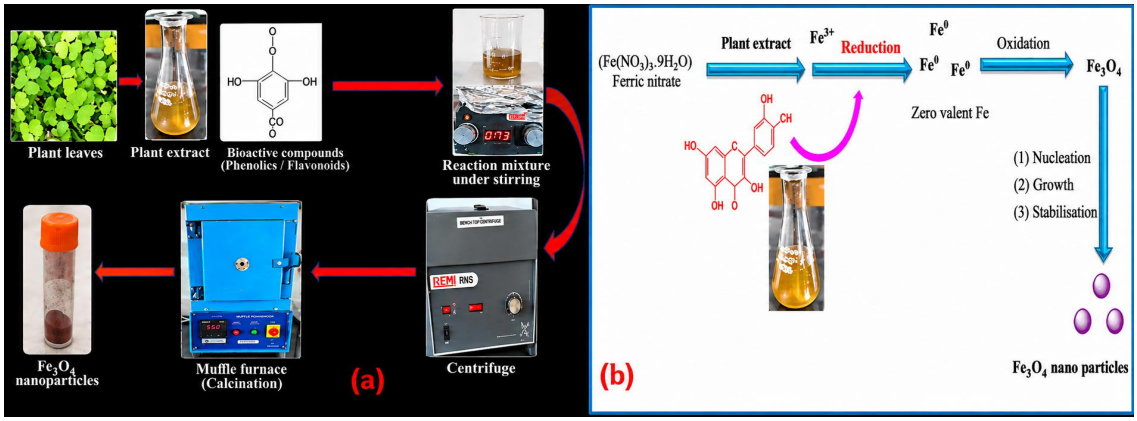

Fig.-1: (a)Visual Depiction of the Environmentally Friendly Synthesis of Fe_3O_4 Nanoparticles from Oxalis Stricta and Ferric Nitrate Nonahydrate. (b)Possible Mechanism of Eco-Friendly Synthesis of Fe_3O_4 NPs

RESULTS AND DISCUSSION

X-ray Diffraction (XRD)

XRD analysis was used to study the crystallinity, phase composition, and particle size of the synthesised nanoparticles. The XRD pattern of the Fe_3O_4 NPs synthesised employing the OSL extract is shown in Fig.2(a). The organic compounds in the plant extract are responsible for reducing ions to iron oxide, confirming the formation of Fe_3O_4 NPs.[20] The diffraction peaks for the plant extract appeared at 30.32°, 35.73°, 43.41°, 53.95°, 57.36°, and 63.06°, corresponding to the planes (220), (311), (400), (422), (511), and (440), respectively. The obtained peak positions were nearly equal to the previously reported values.[21] From the obtained diffraction peaks positions, the synthesised NPs of Fe_3O_4 have a cubic phase and are well matched with the standard magnetite XRD pattern with JCPDS No: 00-019-0629. No additional peaks were observed, further confirming the pure, crystalline nature of Fe_3O_4, indicating the plant-derived phytochemicals are effectively involved in the formation of NPs. The peak with the highest intensity was observed at 35.73°, corresponding to the phase formation of magnetite. The crystallite size of the particles is calculated using the Debye-Scherrer formula.[22]

$$D=\frac{k\lambda}{\beta_{hkl}\cos\theta} \qquad (1)$$

Where D is the crystallite size, k is the crystalline shape factor with Scherer constant=0.9, λ is the wavelength of x-rays (0.154 nm, h, k, l are the Miller indices of the lattice planes, is the half-diffracted angle of the peak, and **β** is the FWHM. Using the above equation, the average crystallite size was 14.37 nm for OSL, which is close to the previously reported value[23], where Fe_3O_4 NPs were synthesised using *Couroupita guianensis Aubl*. fruit extract. The Uniform Deformation Model is applicable for determining crystallite size and strain through the Williamson-Hall model. According to the W-H method, both crystallite size and strain contribute to the widening of diffraction lines. The broadening effect, resulting from strain due to defects and distortions in the crystal, was assessed using a specific formula given by:

$$\epsilon=\frac{\beta}{4\tan\theta} \qquad (2)$$

The broadening caused by lattice strain varies with tanθ; the broadening of diffraction lines attributed to crystallite size is directly related to 1/cosθ. The combined effect of the sample's strain and crystallite size is the total peak broadening and is given by,

$$B_{hkl} = \beta_D + \beta_\varepsilon \qquad (3)$$

After correcting the instrumental broadening, B_{hkl} represents the width at half of the maximum intensity. Using and rearranging equations (1) and (2), we get,

$$B_{hkl}\cos\theta=\frac{k\lambda}{D}+4\varepsilon\sin\theta \qquad (4)$$

The above equation is the same as a linear equation, which is Y = mX + C, where C stands for the Y-intercept and m for the slope. The plot was plotted against 4sinθ on the X-axis and β cosθ on the Y-axis, as shown in Fig. 2 (e). The Y-intercept of the linear fit yields the crystallite size (D), and the slope of the line gives the strain ε. From the W-H plot, the crystallite size and strain are obtained as 8.31nm and 0.0789. The obtained values from the W-H plot are lower than the previously reported values.[24] The different variables related to lattice strain and instrumental broadening in the Scherrer and W–H methods are responsible for the variance in crystallite sizes.

Field-Emission Scanning Electron Microscopy (FESEM)

It is used to study the surface morphology and size of the synthesised Fe_3O_4 Nps. Figures-2(f) and 2(g) show the morphology of the synthesised Fe_3O_4 NPs using *Oxalis stricta* extract, where the nanoparticles exhibit rough and cauliflower structures and a histogram image. This rough, cauliflower-like surface texture is commonly observed during the synthesis of iron oxide Nps due to the presence of biomolecules in the plant extract, which act as reducing and stabilising agents.[25] The formation of larger aggregates may be due to drying or to natural particle affinity. The distribution of the size of the synthesized Nps was roughly estimated using ImageJ software and ranged from 100 nm to 120 nm, and the obtained

values were approximately close to previously reported values.[26] The formation of nanoparticles indicates that the photochemical compounds in the plant extract were responsible for efficient nucleation and development.

Morphological analysis using scanning electron microscopy (SEM) offered valuable insights into the structural characteristics of the nanoparticles. The surface texture observed highlights the influence of phytochemical capping agents present in the leaf extract of *Oxalis stricta*. This biofunctionalisation of the surface helps stabilise the particles and may enhance their biological activity.

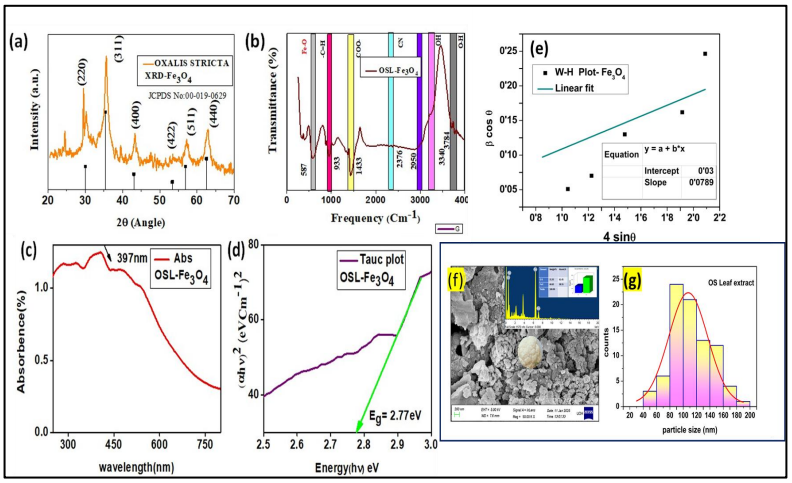

Fig. 2: (a) XRD Patterns of Fe_3O_4 -OSL NPs with the Standard XRD Pattern of JCPDS No: 00-019-0629. (b) FTIR Spectra of Synthesized Fe_3O_4 NPs from *Oxalis Stricta* Leaves Extract (Fe_3O_4 -OSL). (c) UV Spectra of Fe_3O_4-OSL NPs. (d) Tauc Plot Spectra of Fe_3O_4-OSL NPs. (e) W-H plot of Fe_3O_4-OSL NPs. (f) FESEM images of the Fe_3O_4-OSL NPs, with EDAX Spectra Showing Different Elemental Compositions. (g) Histogram of Fe_3O_4-OSL NPs

Fourier Transform Infrared Spectroscopy (FTIR)

FTIR studies provide information about the functional groups present in the sample and further confirm the formation of nanoparticles. Figure-2(b) shows the FTIR spectra of the Fe_3O_4 NPs synthesised using the OSL extracts. The spectra show vibrational bands attributed to various functional groups and confirm the formation of Fe_3O_4 nanoparticles, with capping attributed to phytochemicals in the plant extract. The peak observed at 587 cm^{-1} for OSL-Fe_3O_4[27] corresponds to the Fe-O stretching vibration, confirming the formation of magnetite Nps. The peak at 933 cm^{-1} was assigned to C-H bending vibrations, indicating the presence of plant-derived organic compounds adsorbed on the nanoparticles' surface. The stretching vibrations of carboxylate groups (COO^-) were observed at 1433 cm^{-1}, suggesting the involvement of carboxyl and carbonyl-containing phytochemicals in stabilising the nanoparticles. A weak absorption peak at 2376 cm^{-1} in the extract was assigned to nitrile (C-N) groups, indicating the presence of nitrogen-containing compounds in the plant extract. A weak peak at 2950 cm^{-1} was assigned to the stretching modes of C-H bonds, indicating the presence of organic molecules. The peaks at 3340 cm^{-1} are attributed to O-H stretching vibrations, and the peak at 3784 cm^{-1} for the sample indicates hydroxyl groups from phenolic compounds.[28] Based on the FTIR observations, the study concludes that the plant-mediated phytochemicals play an important role in the bio-generation of Fe_2O_3 nanoparticles, thus adding more credibility to the results. Their potential to possess strong antibacterial activity makes these nanoparticles more suitable and useful in biological (medical), environmental applications.

UV-visible Spectroscopy (UV-Vis)

UV–Vis spectroscopy was used to study the optical properties and to find the band gap of the synthesised nanoparticles. Figure-2(c) shows the UV- visible spectra of the synthesised Fe_3O_4 nanoparticles using the OSL extract between 250 nm and 800 nm. The spectrum shows a prominent peak at 397 nm for Fe_3O_4 synthesized from the OSL extract, indicating the molecular transitions of Fe_3O_4 nanoparticles. This peak was assigned to the electronic transitions between Fe^{2+} and Fe^{3+} ions in Fe_3O_4 (magnetite) and further confirmed the formation of Nps. The peak at approximately 570 nm for OSL- Fe_3O_4 may be due to the phytochemicals present within the plant extract. The decrease in absorption is typical for metal oxide

nanoparticles, indicating no further absorption in the visible to near –infrared region. Electronic transitions play an important role in optical absorption. This depends on the energy gap values. The Tauc equation was used to determine the energy gap values. This is given by the equation $ah\vartheta = A(h\vartheta - E_g)^n$ [29] where 'a' is the absorption coefficient, $h\vartheta$ *is energy* A is a constant, h is Planck's constant, Eg is the energy gap, and n is a constant that takes the values of n=1/2 and n=2 for direct and indirect allowed transitions. In the synthesised Fe_3O_4 nanoparticles using OSL plant extract, mostly the transitions are indirect electronic allowed transitions that take place between O^{2-} to Fe^{3+}. Therefore, the value of n should be taken as 2. The Tauc graph was plotted against energy (hν) on the X-axis and $(\alpha h\nu)^2$ on the Y-axis, as shown in Fig.-2(d). The energy gap is calculated by extrapolating the line from the graph to the X-axis. From the graph, the obtained energy gap value of 2.77 eV is approximately equal to the previously reported value[29] for Fe_3O_4 synthesised from the OSL extract. The formation of Fe_3O_4 Nps is confirmed by the characteristic optical absorption properties observed in the UV-Visible spectroscopy results. The wide absorption seen in the range of UV–visible bands is explained by the presence of Fe^{2+} and Fe^{3+} ions in the spinel crystal structure. The resulting band gap indicates that the nanoparticles have good optical characteristics for use in the field of photocatalysis, environmental purification, sensing and biomedical technologies. In addition, the results of the UV-VIS spectral analysis show that the phytochemicals extracted from the plant actively participate in the green synthesis process, which leads to the stabilisation and reduction of the Fe_3O_4 Nps.

Antifungal Activity

The antimicrobial properties of nanoparticles arise from their tiny size and high ratio of surface area to volume, which effectively envelops the microorganism and limits oxygen availability for respiration. The inhibitory effects of nanoparticles result from the induction of oxidative stress, the release of metal ions, and mechanisms that do not rely on oxidation. Oxidative stress is caused by the formation of various reactive oxygen species, including superoxide (O_2^-), hydroxyl radicals (-OH), singlet oxygen (O_2), and hydrogen peroxide (H_2O_2). Metal oxide nanoparticles have the capability to release metal ions that penetrate through the cell membrane, where they engage with proteins and nucleic acids, causing disruptions in enzyme activity. The antimicrobial properties of iron oxide nanoparticles are associated with their capacity to generate reactive oxygen species (ROS), which cause oxidative stress and harm proteins and DNA in microorganisms. As a strong reducing agent, iron aids in the degradation of functional groups in membrane proteins and lipopolysaccharides. Furthermore, iron nanoparticles trigger oxidation through intracellular oxygen, resulting in oxidative harm via the Fenton reaction.[30,31] These nanoparticles can penetrate compromised membranes, leading to additional damage and ultimately cell death. The mechanism is shown in Fig.-3(a).In this study, the antimicrobial activity of green-synthesised Fe_3O_4 NPs against different fungal and bacterial strains was investigated at different concentrations (0µg/ml,62.5 µg/ml,125 µg/ml,250 µg/ml,500 µg/ml,1000 µg/ml) of Fe_3O_4 NPs. In this study, *A. niger, T. aspratum, S. aureus, and E. faecalis* were used as pathogenic fungal and bacterial strains. This report contradicts previous results, as the synthesized Nps did not show any antibacterial activity but showed antifungal activity at different concentrations in micrograms per millilitre. From the results, it is observed that synthesised Fe_3O_4 NPs show more antifungal activity for *A. Nigar* strain as compared to *T. Asperellum* strain, and the zone of inhibition starts from 125 µg/ml for the OS leaves plant extract shown in Fig. 3 (b) and (c). Figure-3(d) shows the increase in zone size(mm) against *T. Asperellum* bacteria and *A. Nigar*. However, the obtained results are less than the standard PC values, which may be due to their morphology, and the activity may increase by increasing the concentration of the catalyst.

Photocatalytic Activity- Methylene Blue (MB)

This study investigated the photocatalytic efficiency of green-synthesised Fe_3O_4 Nps for the degradation of MB dye under UV radiation. From the Tauc plot, the energy gap of the green-synthesised Fe_3O_4 nanoparticles was 2.77 eV. Because the band gap is narrow, the Fe_3O_4 nanoparticles are able to absorb a sufficient portion of the energy from the UV-Vis source and generate the radicals that degrade the dye. The absorption was carried out by adding 0.05 g of synthesised Fe_3O_4 nanoparticles to 50 mL of

Methylene Blue solution at a concentration of 50 ppm, under stirring under a UV-Vis source and by collecting the samples every 20 min.

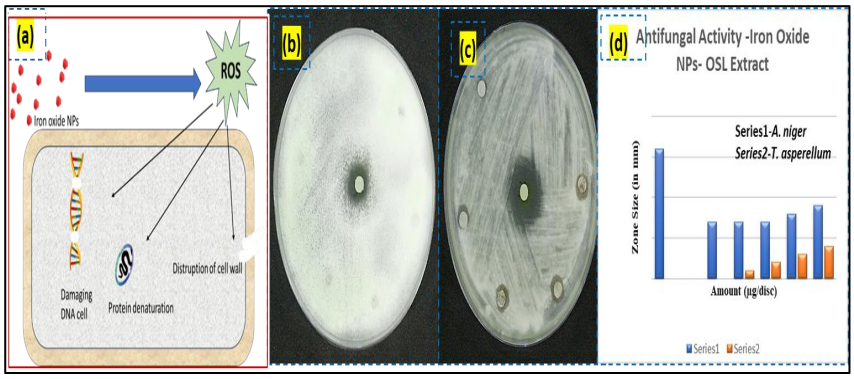

Fig.-3-(a) Basic Mechanism of Antifungal Activity of Fe_3O_4 NPs Nanoparticles, (b) and (c) illustrate the Inhibition Zones for synthesised Fe_3O_4 NPs OSL Extract when Tested against *T. Asperellum* bacteria and *A. Nigar*. (d) Depicts the Differences in Zone Size, measured in mm, for *T. Asperellum* Bacteria and *A. Nigar*.

Before the irradiation of the source, the suspension was stirred in the dark for 1 h to establish adsorption-desorption equilibrium. Then, the UV source was switched on, and this time point was denoted as T=0 min. A suspension of 4-5mL was collected every 20 min, and the collected sample solution was immediately centrifuged to separate the catalyst. The clear solution was analysed using UV-Vis spectroscopy, and a decrease in the absorption peak of Methylene Blue at λ_{max} = 560 nm was observed. The Proposed mechanism is shown in Fig.-4(a).

Mechanism

Photoexcitation

Due to absorption of light energy by the Fe3O4 catalyst, an electron-hole pair is generated in the conduction and valence bands.

$$Fe_3O_4 + h\nu \rightarrow e^-_{CB} + h^+_{VB}$$

Reduction reactions

The electrons in the conduction band reduce oxygen, generating reactive oxygen species (ROS).

$$e^-_{CB} + O_2 \rightarrow \bullet O_2^-$$
$$\bullet O_2^- + H^+ \rightarrow \bullet HO_2$$
$$\bullet 2HO_2 \rightarrow H_2O_2 + O_2$$
$$H_2O_2 + e^-_{CB} \rightarrow \bullet OH + OH^-$$

Oxidation reactions

The holes formed in the valence band oxidise water or hydroxide ions into reactive hydroxyl radicals.

$$h^+_{VB} + H_2O \rightarrow H^+ + \bullet OH$$
$$h^+_{VB} + OH^- \rightarrow \bullet OH$$

Dye Degradation

Both radicals attack the structure of methylene blue, reducing it to smaller structures called intermediates, which are further converted into carbon dioxide and water, along with inorganic gases.

$$MB + \bullet OH\ (or)\ \bullet O_2^- \rightarrow intermediates \rightarrow CO_2 + H_2O + inorganic\ ions$$[19]

The degradation efficiency percentage can be calculated by using the following equation:[24]

$$D(\%) = \frac{C_o - C_f}{C_o} \times 100$$

Where C_o is the initial concentration of the solution, and C_f is the concentration of the solution at time t. The UV-Vis absorption spectra of the Fe_3O_4 NPs synthesised from the OSL extracts of MB dyes and the amount of degradation with time are shown in Fig.-4 (b) and 4(d). According to the graph, the peak intensity of the plant extract at 560 nm corresponded with the strong absorption peak of the MB dye solution, and the peak intensity gradually decreased. A kinetic study was performed to determine the rate constant for the reaction between methylene blue dye and Fe_3O_4 nanoparticles. A pseudo-first-order reaction occurred during the catalytic reduction of the dye molecules. The experimental data were applied to the equation $log\frac{C_f}{C_o} = K_{app}t$[31,32], where k_{app} is the fitted pseudo-first-order model rate constant. A plot of $\ln(C_0/C_f)$ versus time is shown in Fig.-4(c), accounting for the reaction order. The MB reduction rate constant is shown by the slope of the fitted line in the graph. The rate constant for MB degradation was estimated to be 0.0066. The photocatalytic activity confirms the catalytic capacity of the synthesised Fe_3O_4 nanoparticles to remove organic dye contaminants under light irradiation. The results for degradation efficiency and the degradation rate constant indicate that the nanoparticles are promising photocatalysts for water purification and environmental cleanup. This behaviour is explained by photocatalytic activity, which generates reactive oxygen species (ROS) in the aqueous medium, thereby oxidising and decomposing the dye molecules into less harmful products.

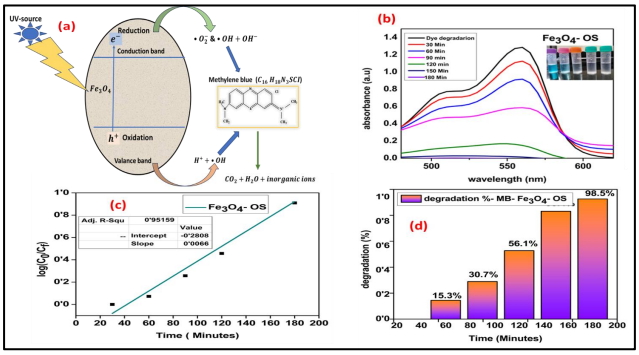

Fig.-4: (a) Possible Explanation for the Photocatalytic Breakdown of MB. (b) Time-Dependent Absorption Spectra of MB in the Presence of the Catalyst. (c) MB Photodegradation Kinetics for OSL. (d) Degradation (%) of MB over Time

CONCLUSION

This study successfully showcased the eco-friendly synthesis of Fe_3O_4 Nps using *Oxalis stricta* leaf extract and ferric nitrate as precursors. The synthesised nanoparticles, characterised by XRD, FESEM, FTIR, and UV-Vis, exhibited a cubic phase with a crystallite size of 6.5 nm and a cauliflower-like morphology. The presence of phytochemicals in the OSL extract played a role in the formation and stabilisation of the nanoparticles. The phytochemicals in *Oxalis stricta* effectively reduced Fe^{3+} ions and stabilised the Fe_3O_4 NPs. Importantly, these green-synthesised Fe_3O_4 NPs displayed promising antifungal activity against *Aspergillus niger* and *Trichoderma asperellum* starting from 125 µg/mL and exhibited efficient photocatalytic degradation of methylene blue dye under UV radiation, following pseudo-first-order kinetics with a rate constant of 0.0066 min^{-1}. This work highlights *Oxalis stricta* as a viable, sustainable bioresource for the production of functional Fe_3O_4 nanoparticles with potential applications in environmental remediation and biomedicine.

The above study demonstrated that green synthesis of Fe_3O_4 nanoparticles is an environmentally benign and sustainable approach. Their strong antibacterial and photocatalytic abilities highlight potential for biomedical and environmental uses, supporting Sustainable Development Goal-3 (Good Health and Well-being).

ACKNOWLEDGMENTS

The authors are thankful for the utilisation of the Photochemical reactor in the Advanced Materials Research Laboratory (AMRL), Department of Physics, Anurag University.

CONFLICT OF INTERESTS

The authors state that there are no conflicts of interest.

AUTHOR CONTRIBUTIONS

The present work is related to *SDG-3: Good Health and Well-Being*. All the authors contributed significantly to this manuscript, participated in reviewing/editing and approved the final draft for publication. The research profile of the authors can be verified from their ORCID ids, given below:

B.Lavanya http://orchid.org/0000-0002-3852-0250
Y. Aparna http://orchid.org/ 0009-0002-3279-6931

Cite this article as: B. Lavanya and Y. Aparn, *Rasayan J. Chem.*, 19(4), 1984-1992(2026), https://doi.org/10.31788/RJC.2026.1949898

REFERENCES

1. K. Andrade-Zavaleta, Y. Chacon-Laiza, D. Asmat-Campos, and N. Raquel-Checca, *Molecules*, **27**, 1367(2022), https://doi.org/10.3390/molecules27041367
2. D.M. Radulescu, V.A. Surdu, A. Ficai, D. Ficai, A.M. Grumezescu, and E. Andronescu, *International Journal of Molecular Sciences*, **24**, 15397(2023), https://doi.org/10.3390/ijms242015397
3. E. Üstün, S.C. Önbaş, S.K. Çelik, M.Ç. Ayvaz, and N. Şahin, *Biointerface Research in Applied Chemistry*, **12**, 2108(2022), https://doi.org/10.33263/BRIAC122.21082116
4. Priya, Naveen, K. Kaur, and A.K. Sidhu, *Frontiers in Nanotechnology*, **3**, 655062(2021), https://doi.org/10.3389/fnano.2021.655062
5. A. Fouhma, N. Tamma, A. Rebiai, and A. Bouafia, *Journal of Sol-Gel Science and Technology*, **115**, 896(2025), https://doi.org/10.1007/s10971-024-06617-0
6. A.N. Amitaye, E.E. Elemike, E. Amitaye, K.M. Al-Ahmary, S.R. Al-Mhyawi, and I. Hossain, *Cleaner Water*, **4**, 100143(2025), https://doi.org/10.1016/j.clwat.2025.100143
7. Z. Shao, Q. Cai, H. Du, H. Hou, J. Sun, and Z. Bao, *Industrial Crops and Products*, **235**, 121631(2025), https://doi.org/10.1016/j.indcrop.2025.121631
8. S. Talebi, *Biological and Molecular Chemistry*, **2**, 253(2024), https://doi.org/10.22034/bmc.2025.521078.1055
9. A.H. Alzaidy, S.H. Ganduh, M.J. Abed, E.A. Dawi, L.S. Jasim, and M.H. Ashoub, *Scientific Reports*, **15**, Article 25743(2025), https://doi.org/10.1038/s41598-025-11532-7
10. M.Y. Darmawan, N.I. Istiqomah, N. Adrianto, R.M. Tumbelaka, A.D. Nugraheni, and E. Suharyadi, *Results in Chemistry*, **6**, 100999(2023), https://doi.org/10.3390/catal14110751
11. M.A. Shabbir, M. Naveed, S.U. Rehman, N.U. Ain, T. Aziz, M. Alharbi, et al., *ACS Omega*, **8**, 33358(2023), https://doi.org/10.1021/acsomega.3c02744
12. P.N. Sannaiah, V.D.P. Alva, and S. Bangera, *Journal of the Iranian Chemical Society*, **19**, 1817(2022), https://doi.org/10.1007/s13738-021-02422-6
13. M. Jamzad and M. Kamari Bidkorpeh, *Journal of Nanostructure in Chemistry*, **10**, 193(2020), https://doi.org/10.1007/s40097-020-00341-1
14. J. Zúñiga-Miranda, J. Guerra, A. Mueller, A. Mayorga-Ramos, S.E. Carrera-Pacheco, C. Barba-Ostria, M. Jaramillo-Vivanco, P. Gómez, and L.P. Guamán, *Nanomaterials*, **13**, 2919(2023), https://doi.org/10.3390/nano13222919
15. M.S. Akhtar, S. Fiaz, S. Aslam, S. Chung, A. Ditta, M.A. Irshad, A.M. Al-Mohaimeed, R. Iqbal, W.A. Al-Onazi, M. Rizwan, and Y. Nakashima, *Scientific Reports*, **14**, 18172(2024), https://doi.org/10.1038/s41598-024-69184-y
16. O. Elkhateeb, M.B. Atta, and E. Mahmoud, *AMB Express*, **14**, 92(2024), https://doi.org/10.1186/s13568-024-01746-9

17. H.S. Devi, M.A. Boda, M.A. Shah, S. Parveen, and A.H. Wani, *Green Processing and Synthesis*, **8**, 38(2019), https://doi.org/10.1515/gps-2017-0145
18. R.A.M.H. Tabrani, G. Antarnusa, and F. Firdaus, *Next Materials*, **8**, 100927(2025), https://doi.org/10.1016/j.nxmate.2025.100927
19. D. Boudouh, R. Ikram, B. Mohamed Jan, H. Simon Cornelis Metselaar, D. Hamana, and G. Kenanakis, *Materials*, **14**, 4306(2021), https://doi.org/10.3390/ma14154306
20. M. Yusefi, K. Shameli, O. Su Yee, S.Y. Teow, Z. Hedayatnasab, H. Jahangirian, et al., *International Journal of Nanomedicine*, **2021**, 2515(2021), https://doi.org/10.2147/IJN.S284134
21. G. Sathishkumar, V. Logeshwaran, S. Sarathbabu, P.K. Jha, M. Jeyaraj, C. Rajkuberan, et al., Artificial Cells, *Nanomedicine, and Biotechnology*, **46**, 589(2018), https://doi.org/10.1080/21691401.2017.1332635
22. Á. de Jesús Ruíz-Baltazar, S.Y. Reyes-López, M. de Lourdes Mondragón-Sánchez, A.I. Robles-Cortés, and R. Pérez, *Results in Physics*, **12**, 989(2019), https://doi.org/10.1016/j.rinp.2018.12.037
23. N. Srivastava, M. Srivastava, A. Alhazmi, A. Mohammad, S. Khan, D.B. Pal, et al., *Scientific Reports*, **11**, Article 24371(2021), https://doi.org/10.1038/s41598-021-03776-w
24. A.V. Ramesh, D. Rama Devi, S. Mohan Botsa, and K. Basavaiah, *Journal of Asian Ceramic Societies*, **6**, 145(2018), https://doi.org/10.1038/s41598-021-03776-w
25. N.A. Yousif, S.M. Al-Jawad, A.A. Taha, and H.H. Abbas, *Journal of Sol-Gel Science and Technology*, **117**, 73 (2026).
26. F. Buarki, H. AbuHassan, F. Al Hannan, and F.Z. Henari, *Journal of Nanotechnology*, **2022**, 5474645 (2022), https://doi.org/10.1155/2022/5474645
27. R. Avilés-Monreal, H.A. Borbón-Nuñez, M.H. Farías, and F. Castillón-Barraza, *SN Applied Sciences*, **5**, Article 389(2023), https://doi.org/10.1007/s42452-023-05611-5
28. D. Khadka, P. Gautam, R. Dahal, M.D. Ashie, H. Paudyal, K.N. Ghimire, et al., *Catalysts*, **14(11)**, 751(2024), https://doi.org/10.3390/catal14110751
29. V. Golthi and J. Kommu, *Hybrid Advance*s, **4**, 100110(2023), https://doi.org/10.1016/j.hybadv.2023.100110
30. R. Hardiyanti, A. Rahmadi, E.Z. Nasution, and A.H. Siregar, *Rasayan Journal of Chemistry*, **19(3)**, 1307(2026), https://doi.org/10.31788/RJC.2026.1936799
31. J.B. Dulla, L.P. Kanchibotla, C.V. Tirupati, S. Boddu, and V.P. Kodali, *Journal of Biochemical Technology*, **16**, 24(2025).
32. J.S.T. Hernandez, A. Aragón-Muriel, W. Corrales Quintero, J.C. Castro Velásquez, N.A. Salazar-Camacho, G.A. Pérez Alcázar, and J.A. Tabares, *Molecules*, **27**, 8976(2022), https://doi.org/10.3390/molecules27248976
33. H. Usha, D. Santhi Priya, J. Chandrasekhar Rao, P. Jayarangarao, P. Sankara Rao, P. Bhadra, and R. Satheesh, *Rasayan Journal of Chemistry*, **19(3)**, 1291(2026), https://doi.org/10.31788/RJC.2026.1939651

[RJC-9898/2026]